Spherical Ruthenium Disulfide-Sulfur-Doped Graphene Composite as An Efficient Hydrogen Evolution Electrocatalyst

Jie Yu,[†] Yanan Guo,[†] Shuanshuan Miao,[†] Meng Ni,[‡] Wei Zhou,[,†] and Zongping Shao[*,†,§]*

[†]Jiangsu National Synergetic Innovation Center for Advanced Materials (SICAM), State Key Laboratory of Materials-Oriented Chemical Engineering, College of Chemical Engineering, Nanjing Tech University, No. 5, Xin Mofan Road, Nanjing 210009, P.R. China

[‡]Building Energy Research Group, Department of Building and Real Estate, The Hong Kong Polytechnic University, Hung Hom, Kowloon, 999077, Hong Kong, China

[§]Department of Chemical Engineering, Curtin University, Perth, Western Australia 6845, Australia

ABSTRACT: The development of high-performance and cost-efficient catalysts to boost hydrogen generation in overall water splitting is crucial to economically obtain green hydrogen energy. Herein, we propose a novel electrocatalyst consisting of spherical RuS_2 on S-doped reduced graphene oxide (s-RuS_2/S-rGO) with high catalytic activity and stability towards hydrogen evolution reaction (HER) in all pH conditions, especially in alkaline electrolytes. RuS_2/S-rGO delivers small overpotentials of 25 and 56 mV at current densities of 10 and 50 mA cm^{-2}, respectively, and a low Tafel slope of 29 mV dec^{-1} with good stability for 100 h in basic solutions. This performance is comparable to and even exceeds that of documented representative electrocatalysts, including the benchmark Pt/C; since the price of Ru is about 1/25th that of Pt, this novel electrocatalyst offers a low-cost alternative to Pt-based HER electrocatalysts. Ruthenium-centred sites of RuS_2 in this hybrid catalyst are responsible for the HER active sites, and S doping in RuS_2 also exerts an important function for the HER activity; density functional theory calculations reveal that the water dissociation ability and adsorption free energy of hydrogen intermediates adsorption (ΔG_{H*}) for RuS_2 are very close to those of Pt. A homemade electrolyser with an s-RuS_2/S-rGO(cathode)//RuO_2/C(anode) couple requires a low voltage of 1.54 V to reach a current density of 20 mA cm^{-2}, while maintaining negligible deactivation over 24-h operation.

KEYWORDS: spherical RuS_2, S-doped reduced graphene oxide, hydrogen evolution reaction, DFT calculations, overall water splitting

1. INTRODUCTION

Hydrogen energy, with its high gravimetric energy density and zero emissions, has been undeniably pursued as one of the most ideal green energy carriers to meet sustainability imperatives.[1-4] Electrochemical water splitting, as a non-fossil fuel-based process, has already attracted copious attention for sustainable hydrogen production.[5-6] The hydrogen evolution reaction (HER) is a pivotal cathodic step in water electrolysis, and it requires active electrocatalysts to promote its sluggish kinetics.[7-8] To date, platinum (Pt)-containing materials are still considered to be the most active HER catalysts at all pH values, but their widespread use is substantially limited by their expensive price, deactivation, and low abundance.[9-11] As a consequence, intensive research efforts have been undertaken towards the development of highly efficient, stable, and low-cost HER catalysts.[10-18] Efficient HER electrocatalysts mainly perform well in acidic media, and only a small percentage of electrocatalysts are active in a wide pH range.[15-16] However, because the most cost-effective oxygen-evolution reaction electrocatalysts (OER) promoting the anodic reaction in electrolysis of water are only available in basic solutions, it is thus highly desirable to develop Pt-free HER catalysts with high efficiency in alkaline media or even in pH-universal solutions.[17-18]

Among the earth-abundant electrocatalysts explored for the HER, transition metal sulfides are a promising class of Pt-free catalysts for the HER.[19, 20] Inspired by the structure/composition of the hydrogenase system, the good activity for HER should stem from metal sulfur clusters with five permanent ligands in a distorted octahedral

ligation shell.[21] Molybdenum disulfide (MoS_2), a typical transition metal sulfide HER electrocatalyst, has attracted the most attention over the past few years.[22-28] It was first confirmed that the HER active sites of semiconducting MoS_2 are mainly edge sites, and thus, various subsequent works have focused on engineering a higher density of edge sites.[2, 22-26] In recent two years, many reports have focused on the comparison and optimization of the HER performance on metallic 1T phase MoS_2 and semiconducting 2H phase MoS_2.[27, 28] Apart from MoS_2, other transition metal sulfides, such as nickel sulfides, cobalt sulfides, iron sulfides, and tungsten sulfides, were also demonstrated to exhibit outstanding HER catalytic performance.[13, 21, 29-33] For example, Faber et al. proposed that cobalt disulfide (CoS_2), with different specific morphologies made available through controlled synthesis, such as films, microwires, or nanowires, plays a key role in determining its overall catalytic efficacy for the HER.[32, 33] Liu et al. prepared a vanadium (V)-doped NiS_2 catalyst where the addition of V led to the electronic structure reconfiguration by engineering vanadium displacement defects, thus contributing to its extraordinary electrocatalytic performance.[13] However, the activities of these catalysts are far lower than those of noble Pt-based catalysts, and most of them perform well only in acidic electrolyte.

Ruthenium disulfide (RuS_2), an unusual metal sulfide, is well-known as one of the most active catalysts for hydrodesulfurization (HDS).[34] Simultaneously, many previous studies have confirmed that a good catalyst for HDS is also a superior HER electrocatalyst due to both reactions relying on reversible binding between the catalyst and hydrogen.[35, 36] Thus, it is anticipated that RuS_2 displays an excellent HER activity.

Ruthenium (Ru), while as one member of the noble metal family, is the cheapest one among them, only with 1/25 price of Pt metal (992 $ per oz).[8, 17] Recently, Ru-based materials, such as RuCo alloys or Ru@C_2N hybrids, have gradually attracted special attention as top hydrogen evolution electrocatalytic materials.[8, 16] Besides, based on RuS_2 as a semiconductor material, the hybridization with nanocarbon materials, such as graphene and carbon nanotube, is a common strategy to further enhance the activity and stability in electrocatalysis, which is widely employed in previously reported articles.[21, 23, 30] Therefore, in this study, we prepared a novel hybrid material of spherical RuS_2 on S-doped reduced graphene oxide (s-RuS_2/S-rGO) by a combined solvothermal sulfidation process and thermal annealing route. As expected, the as-prepared s-RuS_2/S-rGO composite showed the outstanding HER electrochemical activity in solutions with different pH values, which is far more excellent than that of the Ru/rGO catalyst obtained from similar raw materials and better than that of most documented catalysts. More importantly, the HER performance of s-RuS_2/S-rGO in the alkaline solution obviously outperformed benchmark Pt/C, specifically, which is reflected by the lower overpotentials of 25 and 56 mV at the current densities of 10 mA cm^{-2} and 50 mA cm^{-2}, respectively; the smaller Tafel slope value of ~29 mV/decade; and the better stability over 100 h for s-RuS_2/SRG relative to commercial Pt/C catalysts (20 wt.% Pt/C with the overpotentials of 25 and 86 mV at the current densities of 10 mA cm^{-2} and 50 mA cm^{-2}, respectively, and a Tafel slope of ~35 mV/decade; 40 wt.% Pt/C with the overpotentials of 24 and 71 mV at the current densities of 10 mA cm^{-2} and 50 mA cm^{-2}, respectively, and a Tafel slope of ~33 mV/decade). Furthermore, thiocyanate ions

(SCN^-) poisoning studies revealed that the ruthenium-centred sites of RuS_2 in this hybrid catalyst were responsible for the HER active sites, and S doping in RuS_2 also exerted an important function for the HER activity. Notably, pristine RuS_2 is also active enough for HER compared with the noble Pt, and density functional theory (DFT) calculations have disclosed a similar water dissociation ability and similar adsorption free energy of hydrogen intermediates adsorption (ΔG_{H^*}) between them. After hybridization, the improved performance was attributed to enhanced charge transport, increased surface area, and a strong coupling effect between RuS_2 and the S-doped graphene substrate.

2. RESULTS AND DISCUSSION

2.1 Synthesis and characterization of the s-RuS_2/ S-rGO catalyst. The procedure used for the development of the s-RuS_2/ S-rGO catalyst is briefly depicted as follows. A solvothermal synthetic route was first used to synthesize the s-RuS_2/S-rGO precursor (s-RuS_2/S-rGO-p); ruthenium chloride ($RuCl_3$) and L-cysteine as the Ru and S sources, respectively, were dissolved in a mixture of ethylene glycol and DI water containing a certain amount of graphene oxide. The X-ray diffraction (XRD) patterns of s-RuS_2/S-rGO-p in **Figure S1a** revealed its noncrystalline structure. Subsequently, the s-RuS_2/S-rGO-p hybrid was further subjected to annealing treatment to obtain the s-RuS_2/S-rGO hybrid catalyst. For comparison, pure s-RuS_2, metal-free S-rGO, pure rGO, and Ru/rGO catalysts were also synthesized (details of the preparation method for all materials are found in the **Experimental section**).

The crystalline structure of the as-synthesized s-RuS_2/S-rGO composite was first characterized with X-ray diffraction (XRD) measurements, and its corresponding pattern was displayed in **Figure 1a**. The obvious diffraction peaks at 2θ values of approximately 27.5, 31.8, 35.5, 39.3, 45.7 and 54.3° for the s-RuS_2/S-rGO can be well ascribed to the (111), (200), (210), (211), (220), and (311) facets of cubic RuS_2 (JCPDS, No. 73-1677), respectively. Two weak peaks indexed to the (002) and (100) planes of carbon were also detected, which were located at ~25° and ~44°. The XRD patterns of the contrast samples were given in **Figure S1b**.

Shown in **Figure 1b** is the field-emission scanning electron microscopy (FESEM) results of the s-RuS_2/S-rGO hybrid, which revealed the spherical particles with an average diameter of about 1.7 μm (**Figure S2**, which are the RuS_2 particles, as discussed later) covered with S-rGO that exhibited a plate-like and wrinkled morphology. The control experiment without the addition of GO produced pure RuS_2 with a spherical morphology (**Figure S3a**), but the spherical particles vanished in the Ru/rGO catalyst prepared in the absence of S source (**Figure S3b**), suggesting that the S source of L-cysteine instead of GO could be a useful support for mediating the growth of spherical RuS_2 particles. As seen from the transmission electron microscopy (TEM) images of s-RuS_2/S-rGO in **Figure 1c and 1d**, the S-rGO sheets, with the characteristic features of folds and edges, indeed covered the spherical RuS_2 particles. In this structure, S-rGO could act as a bridge to connect the neighbouring RuS_2 microspheres, thereby enhancing the overall electron transfer capability, which ultimately benefitted the electrocatalytic reactions. The high-resolution TEM (HRTEM) patterns of the spherical particles of s-

RuS_2/S-rGO displayed a clear lattice fringe spacing of 0.28 nm (**Figure 1e**), which is consistent with the (200) crystal plane for the cubic RuS_2 phase, further indicating the spherical particles composed of the RuS_2 phase. Notably, through a close observation in the S-rGO area, numerous small clusters (dark spots with an average size of around 5 nm) embedded in the S-doped reduced graphene oxide were observed (**Figure 1f**). The clear lattice fringes with the same distance of about 0.28 nm were also detected for such spots in the HRTEM image (**Inset of Figure 1f**), revealing a small part of the RuS_2 component existing in another morphology. Besides, the further close observations on the edge of S-rGO sheets revealed the reduced graphene oxide with multi-layers and an interlayer separation of 0.34 nm (**Figure 1g**), evidencing the high graphitization. Moreover, high-angle annular dark-field scanning TEM (HAADF-STEM)-EDX line scan and mapping analysis in **Figure 1h-1j** showed a uniform spatial distribution of all elements Ru, S, and C across the marked detection area of the constructed hybrid material. The Ru element content in the hybrid was calculated to be about 38 wt.% from the thermogravimetric analysis (TGA) results (**Figure S4**).

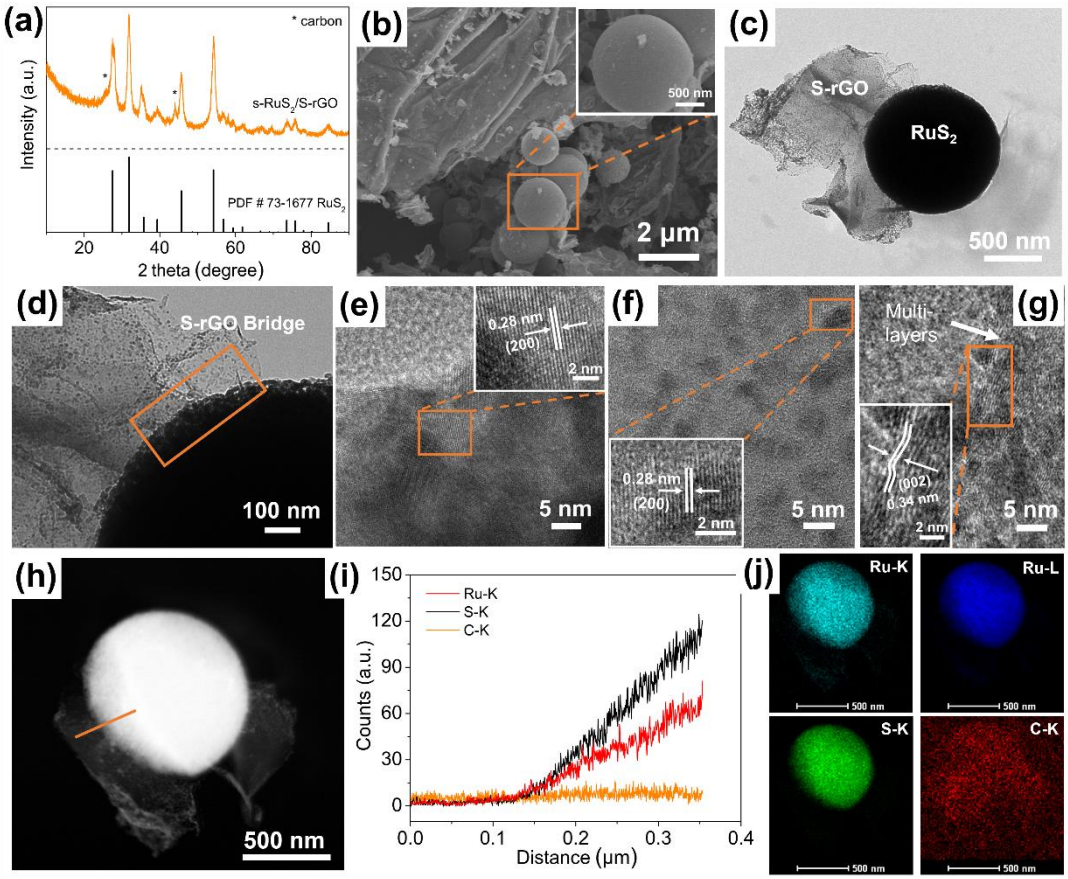

Figure 1. (a) XRD patterns of the as-prepared s-RuS_2/S-rGO composite. The obvious diffraction peaks at about 27.5, 31.8, 35.5, 39.3, 45.7 and 54.3° represent the (111), (200), (210), (211), (220), and (311) planes of cubic RuS_2 (JCPDS, No. 73-1677), respectively. (b) SEM and (c) TEM images of the as-synthesized s-RuS_2/S-rGO catalyst, demonstrating the spherical RuS_2 particle with a diameter of about 1-2 μm covered with S-doped reduced graphene oxide (S-rGO). (d-g) HRTEM images of the s-RuS_2/S-rGO composite. (h) HAADF-STEM image of s-RuS_2/S-rGO with an orange line indicating the line scanning path, and the corresponding (i) line-scanning profile and (j) elemental mapping, which showed a uniform spatial distribution of all elements Ru (cyan, blue), S (green), and C (red).

To investigate the elemental composition and surface chemical state of the s-RuS_2/S-rGO hybrid, X-ray photoelectron spectroscopy (XPS) measurements were performed. The overview survey XPS spectra clearly revealed the concomitance of the Ru, S, C, and adventitious O elements (**Figure S5**). The high-resolution Ru 3p spectrum in **Figure 2a** displayed two main regions of Ru $3p_{1/2}$ and Ru $3p_{3/2}$, which could be fitted to two doublets. A couple of peaks located at 483.7 and 461.4 eV were assigned to the

Ru-S bonds in ruthenium disulfide, and the other two peaks at 486.59 and 463.6 eV correspond to the Ru-O bonds, as stated in previous studies, presumably resulting from a slight superficial oxidation process occurring upon exposing to air for RuS_2.[30, 37] In the high-resolution S 2p spectrum (**Figure 2b**), the two peaks at the low binding energy of 163.03 (S $2p_{1/2}$) and 161.85 eV (S $2p_{3/2}$) were related to the sulfide signal (Ru-S), while the peak of -C-S-C- confirmed the successful doping of sulfur atoms into the carbon framework.[38, 39] Besides, the presence of the S oxidation state (167.97 eV) further explains the surface oxidation.[38] Notably, a peak positive shift was observed from 483.7 eV for Ru $3p_{1/2}$ of RuS_2 to 483.2 eV for Ru $3p_{1/2}$ of metallic Ru, while there was also a peak negative shift from 163.03 eV for S $2p_{1/2}$ of RuS_2 to that of the S element (163.9 eV). These results indicate that Ru atoms in the RuS_2 are positively charged, while S atoms are negatively charged, revealing the electron transfer from Ru to S. Thus, the Ru atom was easy to trap negatively charged hydride and the S atom can easily trap positively charged proton during hydrogen production process, which should be good for the HER.[6] More significantly, the peak assigned to the Ru-S bonds for s-RuS_2/S-rGO was deviated from that for a physical mixture of s-RuS_2 and S-rGO (s-RuS_2+S-rGO, in which the mass ratio of RuS_2 is the same as that of the s-RuS_2/S-rGO hybrid.) (**Figure S6**), directly representing the electron interaction at the interface between s-RuS_2 and S-rGO of the s-RuS_2/S-rGO sample, as reported by the previous article.[15] Additionally, the Raman spectrum analysis of the RuS_2/S-rGO hybrid was conducted to characterize carbon component (**Figure 2c**). Obviously, the RuS_2/S-rGO hybrid exhibited three Raman peaks centered at approximately 1350, 1591 and 2694

cm^{-1}, corresponding to the D, G, and 2D bands, respectively.[16] The I_D/I_G band intensity ratio is about 1.12, implying the existence of a large number of defects in the s-RuS_2/S-rGO hybrid, further confirming that large amounts of S atoms were doped into the carbon framework. Meanwhile, the broad and weak 2D band suggests that the carbon skeleton is thin graphene with several layers, thus supporting the TEM analysis.[40] Moreover, the peak representative of the G band clearly shifted from 1575 cm^{-1} for S-rGO to 1590 cm^{-1} for s-RuS_2/S-rGO (**Figure S7**), which also evidences the strong interaction between RuS_2 and S-rGO in the compound.[38] When the Raman shift was below 1000 cm^{-1} for s-RuS_2/S-rGO (**Figure S7**), a broad peak ranging from ~ 350 cm^{-1} to ~405 cm^{-1} was observed, which should be assigned to Ru-S bonds, as previous reports. [41] Based on the N_2 adsorption-desorption isotherms (**Figure 2d**), the specific surface area of s-RuS_2/S-rGO was measured to be 53 $m^2\ g^{-1}$, and its pore size distribution is centered at about 3.7 nm (**Figure 2d** and **Table S1**).

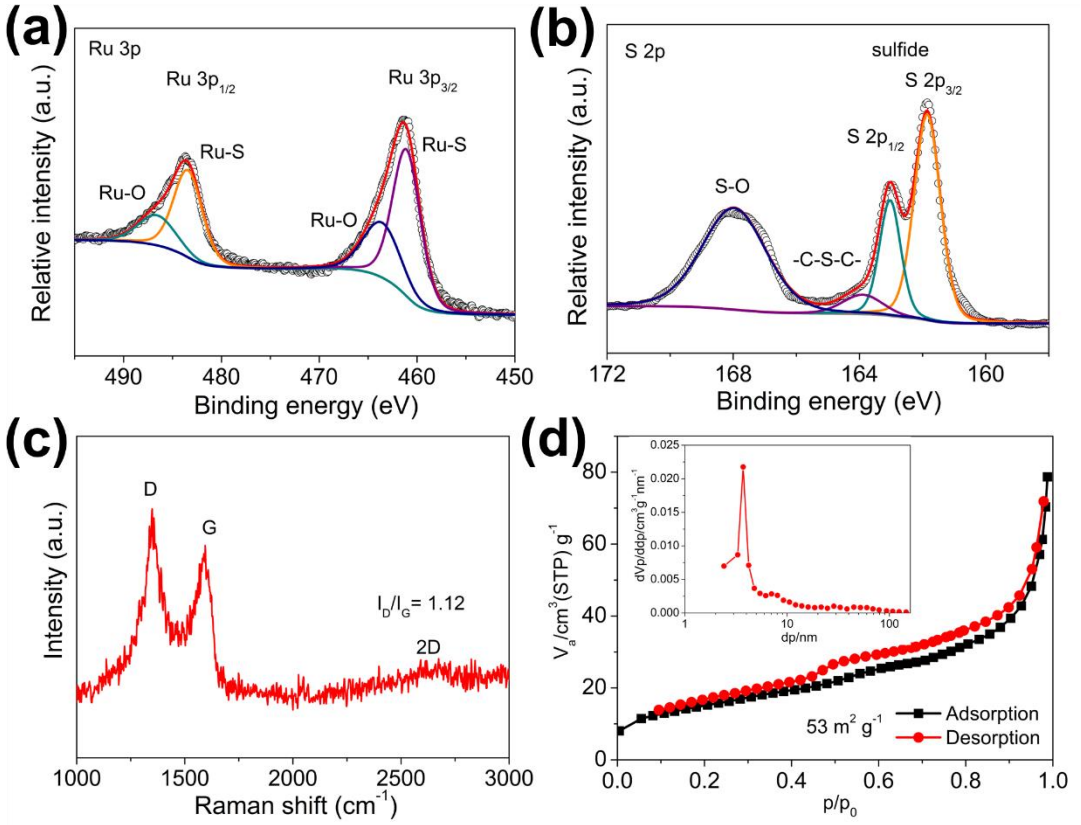

Figure 2. (a, b) High-resolution XPS spectra of Ru 3p and S 2p, (c) Raman spectrum, and (d) N_2 adsorption-desorption isotherm of the the as-prepared s-RuS_2/S-rGO composite (the insert is the corresponding pore size distribution plot).

2.2 Electrocatalytic HER performance in alkaline media. The electrocatalytic HER activity of the s-RuS_2/S-rGO hybrid and reference samples, including the bare glassy carbon (GC), metal-free S-rGO, s-RuS_2/S-rGO-p, pure s-RuS_2 and a physical mixture of s-RuS_2 and S-rGO (s-RuS_2+S-rGO), was first comparatively investigated in an Ar-saturated 1 M KOH aqueous solution by using a three-electrode set-up. **Figure 3a** displayed their polarization curves with iR correction. Besides, for the sake of more accurate and objective comparison, **Figure S8** listed the overpotentials at the different current densities of 10 and 50 mA cm^{-2} for these catalysts, respectively, which were shown in the form of scatter diagram with error bars. The bare GC had no contribution to the HER activity, and the HER activity of the s-RuS_2/S-rGO-p hybrid was extremely

poor, as indicated by a large overpotential of 421 mV at the representative current density of 10 mA cm^{-2} (η_{10}). In sharp contrast, the as-prepared s-RuS_2/S-rGO sample exhibited remarkable HER performance only with 25 mV of η_{10}, which was much lower than those of pure s-RuS_2 (η_{10} = 40 mV) and S-rGO (η_{10} = 555 mV), indicating the synergistic effect between s-RuS_2 and S-rGO. Of note, the HER performance of pure s-RuS_2 was also excellent relative to most of the reported catalysts, and it largely outperformed that of S-rGO, revealing that the RuS_2 phase is dominantly responsible for the high HER activity. Moreover, although S-rGO showed the negligible HER performance, S doping still resulted in an improved HER activity compared to pure rGO (**Figure S9**), which were likely attributed to defects around dopant atoms as favorable sites, corresponding to previous reports.[42, 43] More specifically, the enhanced performance stemming from the synergistic effect between s-RuS_2 and S-rGO for the s-RuS_2/S-rGO hybrid could be attributed to the following aspects: (1) the RuS_2 phase is considered as the main active phase; (2) the introduction of rGO can improve the charge transport, as reflected by the electrochemical impedance spectroscopy (EIS) (**Figure S10**), and increase the surface area compared to pure s-RuS_2 **(Table S1**); (3) the strong coupling is created between s-RuS_2 and S-rGO, which is demonstrated by comparing the HER activities of s-RuS_2/S-rGO and s-RuS_2+S-rGO **(Figure 3a)**, and the larger electrochemically active surface area (ECSA) of s-RuS_2/S-rGO relative to s-RuS_2+S-rGO suggests the exposure of more active sites (**Figure S11**). Accordingly, the HER kinetics of s-RuS_2/S-rGO were consistently enhanced by comparing their Tafel plots (**Figure S12**). The smallest Tafel slope of s-RuS_2/S-rGO among them indicates

the most rapid rise in the hydrogen evolution rate along with the increased impressed voltage, demonstrating the most excellent performance displayed in the HER polarization curves **(Figure 3a)**.

A metallic Ru/rGO composite catalyst (the mass content of Ru: ~56 wt. %, **Figure S13**) and the commercial Pt/C catalysts (including 20 wt.% and 40 wt.% Pt/C) were also measured for further comparison. As shown in **Figure 3b**, s-RuS_2/S-rGO afforded the remarkable HER activity with low overpotentials of 25 and 56 mV to reach current densities of 10 (η_{10}) and 50 mA cm^{-2} (η_{50}), respectively, which are obviously better than those of the Ru/rGO composite (48 and 109 mV, respectively). Moreover, the η_{10} value of s-RuS_2/S-rGO is equal to that of 20 wt.% Pt/C, and only 1 mV larger than that of 40 wt.% Pt/C (24 mV). Most importantly, the fast HER kinetics enable the s-RuS_2/S-rGO catalyst to obtain an η_{50} value as low as 56 mV, largely outperforming the 20 wt.% and 40 wt.% Pt/C catalysts (86 and 71 mV, respectively). Besides, as compared to the commercialized Ir and Ru oxides, the s-RuS2/S-rGO catalyst exhibited obviously superior HER activity (**Figure S14**). Shown in **Figure 3c** are Tafel plots of these samples that may provide the kinetic evaluation of HER. Tafel slopes of 29, 30, 35, and 33 mV dec^{-1} were obtained for the s-RuS_2/S-rGO composite, the Ru/rGO composite, and the commercial two Pt/C catalysts (20 wt.% and 40 wt.% Pt/C), respectively. This reveals that hydrogen generation over s-RuS_2/S-rGO proceeds with the fastest kinetics through a Volmer-Tafel mechanism wherein the electrochemical desorption of H_2 serves as the rate-determining step.[44] By extrapolating the Tafel plots, the value of the exchange current density (j_0) of s-RuS_2/S-rGO was calculated to be 1.32 mA cm^{-2},

which was 2.5 times larger than that of the Ru/rGO composite (0.51 mA cm^{-2}) and comparable to the 20 wt.% and 40 wt.% Pt/C catalysts (2.04 and 1.9 mA cm^{-2}, respectively), highlighting the remarkable H_2 evolution efficiency of the s-RuS_2/S-rGO catalyst.[8] **Figure 3d** displayed a straightforward comparison among the four catalysts by listing the corresponding η_{10}, η_{50} and j_0. It is worth noting that such excellent electrocatalytic activities, i.e., the small overpotential, low Tafel slope, and high exchange current density of s-RuS_2/S-rGO, make it rank at the best HER electrocatalytic materials in basic electrolytes **(Table S2)**. Given that only a few transition metal sulfides as the HER electrocatalysts in the alkaline solution have been reported, **Figure 3e** showed the η_{10} and Tafel slopes of s-RuS_2/S-rGO, along with these reported transition metal sulfides electrocatalysts, including $Ni_xCo_{3-x}S_4$/Ni_3S_2/NF, NiS_2-NF-A, CoS_2/Ti foil, MoS_2/Mo foil, CoMoS-24h, MoS_2-Ni_3S_2 HNRs/NF, MoS_2/NF, Ni_3S_2/NF, NiS_2/MoS_2, NiS_2, CP/CTs/Co-S, NiS_2HMSs, and MoS_{2+x}, in a 1 M KOH solution.[45-53] Markedly, the catalytic activity of s-RuS_2/S-rGO towards hydrogen evolution was much better than those of other reported sulfide electrocatalysts. More attractively, Ru is more economically viable than commercial Pt, where the price activity of s-RuS_2/S-rGO with 147 and 730 A per dollar generated at overpotentials of 50 and 100 mV, respectively, was over 30 and 58 times larger than that of 40 wt.% Pt/C, respectively, and was over 19 and 37 times larger than that of 20 wt.% Pt/C, respectively (**Figure S15**).

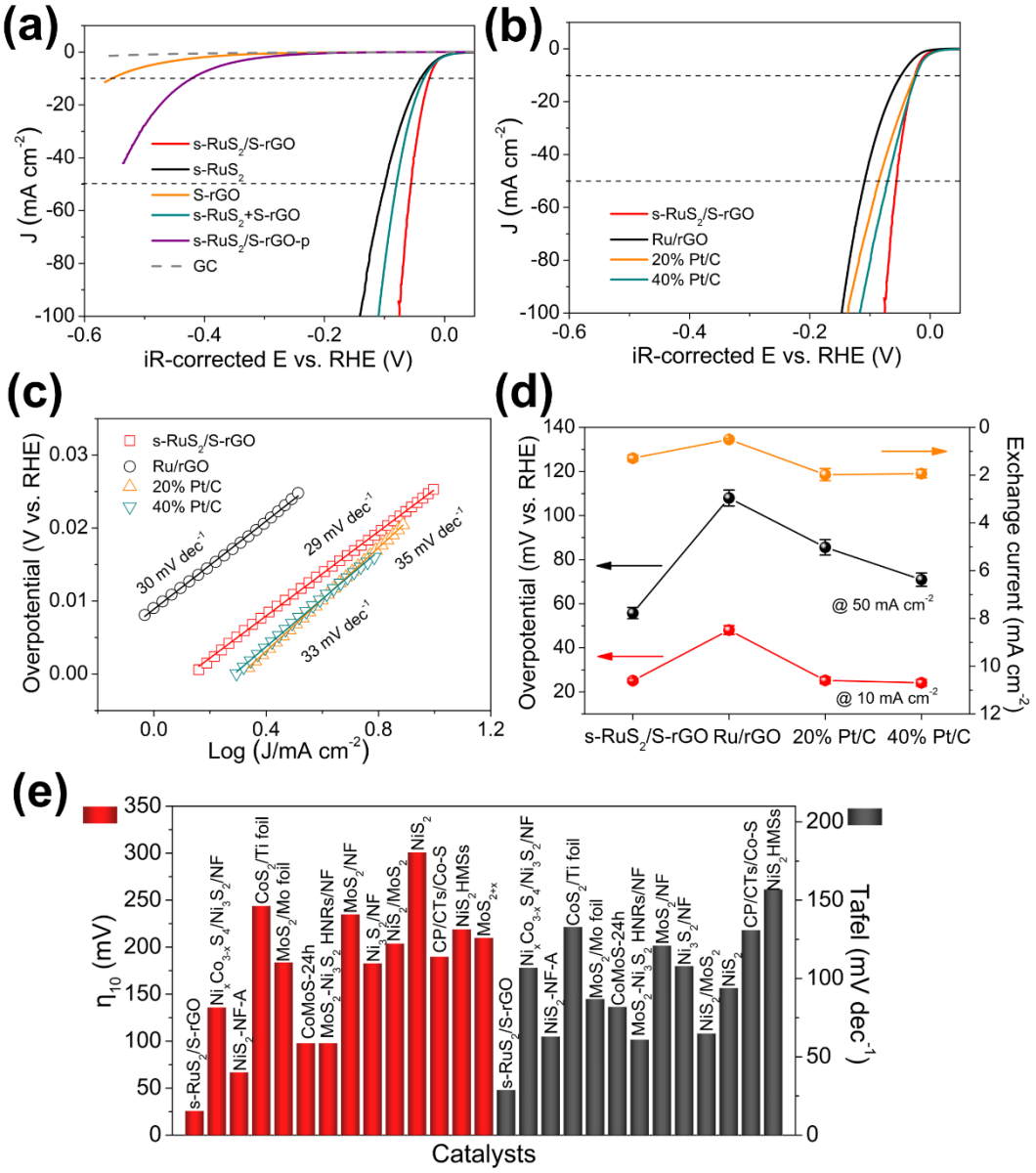

Figure 3. (a) HER polarization curves of the s-RuS_2/S-rGO hybrid and reference samples, including the bare GC, metal-free S-rGO, s-RuS_2/S-rGO-p, pure s-RuS_2, and s-RuS_2+S-rGO in 1 M KOH with a scan rate of 5 mV s^{-1}. (b) HER polarization curves in 1 M KOH with a scan rate of 5 mV s^{-1}, (c) the corresponding Tafel plots, and (d) comparison of the overpotentials at different current densities (10 mA cm^{-2} and 50 mA cm^{-2}, respectively) (left) and exchange current densities (right) of the s-RuS_2/S-rGO hybrid, Ru/ rGO composite, and the commercial two Pt/C catalysts (20 wt.% and 40 wt.% Pt/C). Error bars represent standard deviations from at least three independent measurements. (e) Overpotentials at a current density of 10 mA cm^{-2} and Tafel slopes of s-RuS_2/S-rGO and these reported transition metal sulfides in the 1 M KOH aqueous solution.

Electrochemical durability is another critical parameter for evaluating an HER catalyst. A long-term cycling test was first carried out for as-prepared s-RuS_2/S-rGO.

Comparing the polarization curves before and after 1000 continuous cyclic voltammetry (CV) sweeps in a 1 M KOH solution, the final polarization curve showed nearly no difference from the initial one (**Figure 4a**), indicating a superior stability of s-RuS_2/S-rGO under the operating conditions. In addition, **Figure 4b** depicted a time-dependent potential change at three fixed current densities, namely, 10 mA cm^{-2}, 20 mA cm^{-2}, and 50 mA cm^{-2}, respectively, for both s-RuS_2/S-rGO and 20 wt.% Pt/C catalysts. These tests were performed with a high catalyst loading of 2 mg cm^{-2} on carbon cloth. Clearly, in these tests, these potentials showed no obvious attenuation during the 100-h test for the s-RuS_2/S-rGO sample, even at a high current density of 50 mA cm^{-2} or for longer time (~ 200 h) (**Figure S16**), while the potentials for Pt/C underwent rapid degradation with time, further evidencing the prominent stability of our developed material. The poor stability of Pt/C might be attributed to the agglomeration of Pt nanoparticles, dissolution of Pt surface atoms, and corrosion of the carbon support.

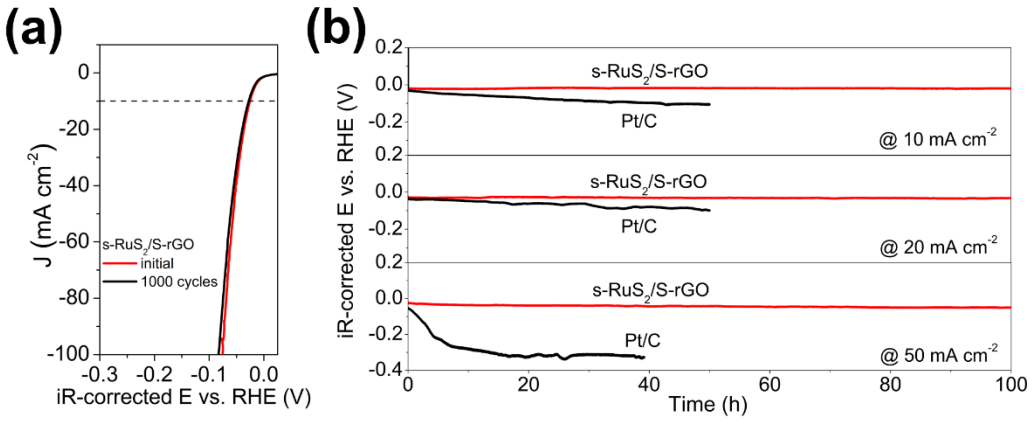

Figure 4. (a) HER polarization curves of the s-RuS_2/S-rGO sample initially and after 1000 cycles in basic media. (b) Time-dependent potential changes at three fixed current densities of 10 mA cm^{-2}, 20 mA cm^{-2}, and 50 mA cm^{-2}, respectively, for these s-RuS_2/S-rGO and 20 % Pt/C catalysts in alkaline media.

2.3 Electrocatalytic HER performance over a wide pH range. Given that there are various types of water splitting devices, a desired HER catalyst should work well over a wide pH range. Thus, we further evaluated the HER performance of the s-RuS_2/S-rGO hybrid and the control samples in acidic and neutral media. The s-RuS_2/S-rGO compound exhibited a η_{10} of 69 mV and a Tafel slope of 64 mV dec^{-1} in 0.5 M H_2SO_4 electrolytes (**Figure S17**). A slight higher η_{10} of 93 mV and smaller Tafel slope of 41 mV dec^{-1} were required for the s-RuS_2/S-rGO catalyst operating in a 1 M PBS solution (**Figure S18**). These values demonstrate its good catalysis behavior, which is comparable to that of commercial Pt/C catalysts and much better than other control samples in **Figure S14**, **S17**, and **S18**. Moreover, these values compare favourably with those of most reported HER catalysts used under similar conditions, as listed in **Table S3.**

2.4 Investigation of the active sites and calculation of TOF. It is well-known that thiocyanate ions (SCN^-) can make metal-centred catalytic sites poisoned. [54] Aiming at gaining more insight into the nature of the active sites of the s-RuS_2/S-rGO hybrid catalyst, the HER activity tests of the s-RuS_2/S-rGO and S-rGO samples were also performed in a 1 M KOH electrolyte with 10 mM SCN^-. As depicted in **Figure 5a**, the η_{10} of the s-RuS_2/S-rGO hybrid significantly increased from 25 mV to 96 mV, and a decrease in the current density by more than 90 % was also observed at the overpotential of 50 mV in the presence of SCN^- ions, indicating the blocking of active sites. In sharp contrast, the initial HER polarization curve of the S-rGO catalyst is completely overlapped with that after the addition of SCN^- ions (**Figure 5b**), revealing

that SCN^- ions have no effect on the HER activities of the metal-free S-rGO catalyst. These results strongly confirmed that the ruthenium-centred sites of RuS_2 are the active sites of the s-RuS_2/S-rGO hybrid catalyst. However, the higher HER activity of RuS_2 relative to its metallic counterpart is believed to result from the effect of S atoms, in which S with more electronegativity can regulate the electron distribution around the Ru atoms, which is directly demonstrated by the aforementioned XPS analysis results. This is similar to metal complex catalysts and hydrogenases.[6] Thus, for RuS_2, the Ru and basic S atoms play the roles of the hydride-acceptor and proton-acceptor centers, respectively, benefiting hydrogen production. In a word, the S in RuS_2 could promote the formation of the hydride at the ruthenium-centred sites for subsequent hydrogen evolution via electrochemical desorption during cathodic polarization. Thus, the S atoms in RuS_2 are also responsible for the HER performance.

Based on having understood the active origin of the s-RuS_2/S-rGO catalyst, the turnover frequency (TOF) value for each active site of this catalyst was roughly estimated, which is an important figure of merit employed to appraise the intrinsic catalytic performance of an electrocatalyst. The specific calculation process is given in **Note S1**. As the benchmark HER catalyst, Pt displayed the TOF values of 0.47 and 0.95 s^{-1} at overpotentials of 25 and 50 mV, respectively, in the 1 M KOH electrolyte.[8] To reach these TOF values of 0.5 and 1 s^{-1}, the s-RuS_2/S-rGO catalyst needed overpotentials of 40 mV and 56 mV, respectively, which is comparable to the recently reported Ru@C_2N catalyst and much larger than that required for other typical reported HER electrocatalysts in the same electrolyte, such as Ru/C_3N_4/C, CP/CTs/Co-S, NiMo

alloy, Ni-C-N, Ni_2P, Ni_5P_4, γ-Mo_2N, and α-Mo_2C, shown in **Figure 5c**.[17, 51, 55-58]

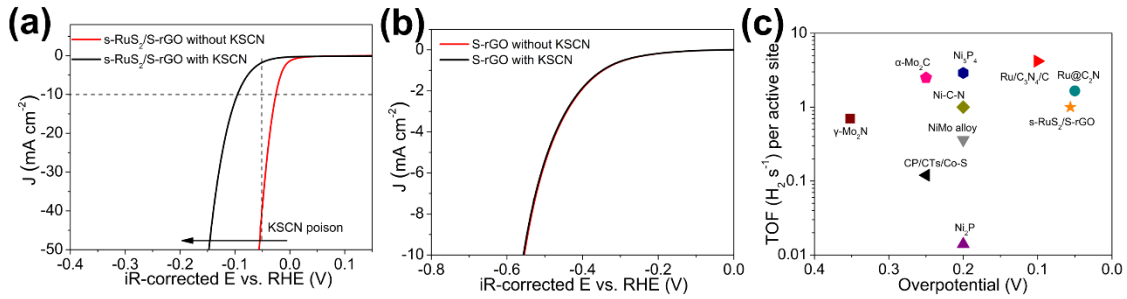

Figure 5. (a, b) HER polarization curves of the s-RuS_2/S-rGO and S-rGO samples with and without 10 mM KSCN in 1 M KOH. (c) TOF values of the s-RuS_2/S-rGO sample and other typical reported HER electrocatalysts in 1 M KOH.

2.5 DFT calculations. To examine the HER catalytic behavior of individual RuS_2 in alkaline electrolytes, DFT calculations were performed for the water dissociation reaction and the adsorption of hydrogen intermediates; **Note S2** showed the specific calculation process. According to our HRTEM and XRD results, the RuS_2 (200) surface is the dominant crystal surface exposed in the synthesized material; therefore, this surface was modelled as the representative in the current study. For comparison, the $\sqrt{3} \times \sqrt{3}$ reconstructed Pt (111) surface, Ru (001) surface and RuO_2 (110) surface were also computed, considering the fact that they are among the most commonly detected and the most representative ones both experimentally and theoretically. [17, 59] The calculated adsorption free energy of hydrogen intermediates (ΔG_{H*}, a common descriptor in the HER) and the energy barrier for breaking the OH-H bond in water (ΔE) on the Pt (111) surface (see **Figure S19a**) are very similar to previous studies, [17, 60] confirming the validity of the current DFT method. As shown in **Figure 6**, the ΔE is 1.13 eV on the RuS_2 (200) surface, which is comparable to that on the Pt (111) surface (**Figure S19a**). This indicates that the RuS_2 surface has a similar ability of promoting

water dissociation with the Pt surface. The computed ΔG_{H^*} on the RuS_2 (200) surface is 0.16 eV, which is quite close to the optimal value ($\Delta G_{H^*} = 0$) and that of the benchmark Pt (**Figure S19b**). This means that the hydrogen adsorption on the RuS_2 surface is neither too weak nor too strong. Therefore, the RuS_2 surface shows a comparable water dissociation ability to that of the Pt surface, and both hydrogen adsorption and desorption easily occur on this surface.

As seen from **Figure S19** and **Figure 6a**, the energy barrier for breaking the OH-H bond in water on the RuS_2 (200) surface ($\Delta E = 1.13$ eV) is close to that on Ru (001) ($\Delta E = 0.72$ eV), but much higher than that on RuO_2 (110) ($\Delta E = 0.03$ eV). Hence, from the kinetic point of view, RuO_2 exhibits the fastest water dissociation among the three materials, which should be favorable to hydrogen evolution. However, it is noteworthy that in the next step of H adsorption process, RuS_2 (200) surface shows the smallest adsorption free energy ($\Delta G_{H^*} = 0.16$ eV) among them, and it is largely lower than that on RuO_2 (110) ($\Delta G_{H^*} = 0.84$ eV). Thus, from the thermodynamic viewpoint, conversely, RuS_2 is the most active towards H_2 production. Nevertheless, for the overall reaction, the two steps synergistically determine the catalytic results, none of which is dispensable, thus contributing to the different HER catalytic behaviors for the different catalysts in **Figure 3b** and **Figure S14a**.

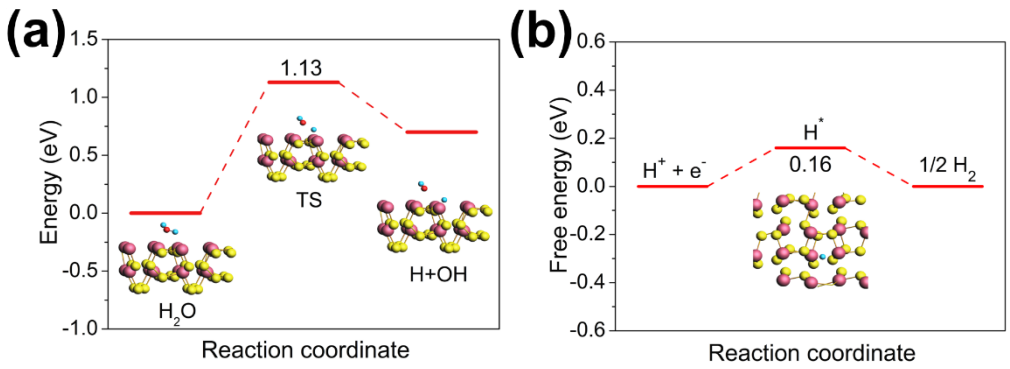

Figure 6. (a) The energy diagram of the water dissociation on the RuS_2 (200) surface. The geometries of the initial state (H_2O), the transition state (TS) and the final state (H+OH) are shown. (b) The adsorption free energy of hydrogen intermediates adsorption (ΔG_{H*}) on the RuS_2 (200) surface. The Ru, S, H, and O atoms are represented by pink, yellow, blue and red balls, respectively.

2.6 Overall water electrolysis. Given the above HER results, the s-RuS_2/S-rGO hybrid as a cathode catalyst was paired with the RuO_2/C catalyst as an anode catalyst to assemble a closely practical water electrolyzer operated in basic media (1 M KOH). As a benchmark, the Pt/C(cathode)//RuO_2/C(anode) couple was configured as a reference. All the catalysts were loaded onto the same-sized Ni foams, and the mass loading was 5 mg cm^{-2}. Obviously, the bare Ni foam// Ni foam made a negligible contribution to the overall water-splitting performance, shown in **Figure 7a**. When operating at the voltage of less than 1.65 V, the s-RuS_2/S-rGO//RuO_2/C pair displayed a comparable activity to that of the Pt/C//RuO_2/C benchmark combination. To reach a current density of 20 mA cm^{-2}, an electrolyzer voltage of 1.54 V was required for the s-RuS_2/S-rGO//RuO_2/C couple. When the applied voltage is higher than 1.65 V, the water-splitting current density of s-RuS_2/S-rGO//RuO_2/C couple increases rapidly and strongly surpasses that of Pt/C//RuO_2/C. In addition, the long-term electrolyzer stability test was conducted at a current density of 20 mA cm^{-2} for the s-RuS_2/S-rGO//RuO_2/C couple. As revealed in **Figure 7b,** a little voltage loss of the electrolyzer after 24 h

continuous operation was achieved, suggesting the outstanding robustness of our catalyst.

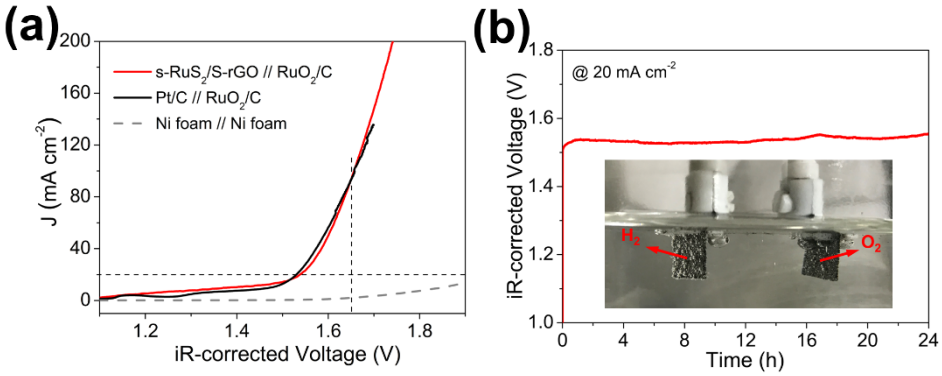

Figure 7. (a) Polarization curves of s-RuS_2/S-rGO(−)//RuO_2/C(+), Pt/C(−)//RuO_2/C(+), and bare Ni foam//Ni foam for overall water splitting in 1 M KOH with a mass loading of 5 mg cm^{-2}. (b) The corresponding chronopotentiometric curve of the s-RuS_2/S-rGO(−)//RuO_2/C(+) couple at a constant current density of 20 mA cm^{-2} in 1 M KOH. The inset is an optical image of the H_2 and O_2 bubble generation by the homemade water electrolyzer driven by a AAA battery with a nominal voltage of 1.5 V.

3. CONCLUSIONS

To summarize, a novel hybrid of spherical RuS_2 on S-doped reduced graphene oxide (s-RuS_2/S-rGO) was fabricated via a tandem solvothermal sulfidation and thermal annealing strategy, and it displayed prominent HER catalytic performance in the wide pH range of 0-14. In particular, the HER activity and stability of s-RuS_2/S-rGO in alkaline media, characterized by the low η_{10} and η_{50} of 25 and 56, a small Tafel slope of 29 mV dec^{-1} and the stable continuous 100-h operation, even exceed the performance of benchmark Pt/C catalysts, ranking one of these most active electrocatalysts towards HER in alkaline solutions ever reported. The high HER performance was mainly attributed to the RuS_2 species, and DFT calculations also indicate a similar water dissociation ability and the adsorption free energy of hydrogen intermediates adsorption (ΔG_{H^*}) between RuS_2 and Pt. Furthermore, in situ

hybridization with GO contributed to the enhanced charge transport, increased surface area and a strong coupling interaction between the RuS_2 and S-doped graphene matrix, thus further promoting the HER activity. The catalyst in this study is not only suitable for hydrogen production from water splitting, but also can be extended to other energy-related processes, such as metal-air batteries, fuel cells, CO_2 reduction, and so on.

ASSOCIATED CONTENT

Supporting Information

The Supporting Information is available free of charge on the ACS Publications website. Experimental section (including the detail materials synthesis process), various characterization results (XRD, SEM, TG, XPS, and Raman), HER electrochemical data, and DFT calculation details.

AUTHOR INFORMATION

Corresponding Author

*E-mail: zhouwei1982@njtech.edu.cn (Wei Zhou). Tel.: +86 25 83172256; Fax: +86 25 83172242.

*E-mail: shaozp@njtech.edu.cn (Zongping Shao). Tel.: +86 25 83172256; Fax: +86 25 83172242.

Notes

The authors declare no competing financial interest.

ACKNOWLEDGMENTS

This study was financially supported by the Jiangsu Natural Science Foundation for

Distinguished Young Scholars (No. BK20170043), the National Nature Science Foundation of China (No. 21576135), and the Youth Fund in Jiangsu Province (No. BK20150945). In addition, we are grateful to the High Performance Computing Center of Nanjing Tech University for supporting the computational resources.

REFERENCES

(1) Dresselhaus, M. S.; Thomas, I. L. Alternative Energy Technologies. *Nature* **2001**, *414*, 332-337.

(2) Deng, J.; Li, H.; Wang, S.; Ding, D.; Chen, M.; Liu, C.; Tian, Z.; Novoselov, K. S.; Ma, C.; Deng, D.; Bao, X. Multiscale Structural and Electronic Control of Molybdenum Disulfide Foam for Highly Efficient Hydrogen Production. *Nat. Commun.* **2017**, *8*, 14430.

(3) Crabtree, G. W.; Dresselhaus, M. S.; Buchanan, M. V. The Hydrogen Economy. *Phys. Today* **2004**, *57*, 39-44.

(4) Zhang, Y.; Zhou, Q.; Zhu, J.; Yan, Q.; Dou, S. X.; Sun, W. Nanostructured Metal Chalcogenides for Energy Storage and Electrocatalysis. *Adv. Funct. Mater.* **2017**, *27*, 1702317.

(5) Zeng, K.; Zhang, D. Recent Progress in Alkaline Water Electrolysis for Hydrogen Production and Applications. *Prog. Energy Combust. Sci.* **2010**, *36*, 307-326.

(6) Tian, J.; Liu, Q.; Asiri, A. M.; Sun, X. Self-Supported Nanoporous Cobalt Phosphide Nanowire Arrays: An Efficient 3D Hydrogen-Evolving Cathode over the Wide Range of pH 0-14. *J. Am. Chem. Soc* **2014**, *136*, 7587-7590.

(7) Shi, Y.; Zhang, B. Recent Advances in Transition Metal Phosphide Nanomaterials: Synthesis and Applications in Hydrogen Evolution Reaction. *Chem. Soc. Rev.* **2016**, *45*, 1529-1541.

(8) Mahmood, J.; Li, F.; Jung, S.; Okyay, M. S.; Ahmad, I.; Kim, S.; Park, N.; Jeong, H. Y.; Baek, J. -B. An Efficient and pH-Universal Ruthenium-Based Catalyst for the Hydrogen Evolution

Reaction. *Nat. Nanotechnol.* **2017**, *12*, 441-447.

(9) McKone, J. R.; Warren, E. L.; Bierman, M. J.; Boettcher, S. W.; Brunschwig, B. S.; Lewis, N. S.; Gray, H. B. Evaluation of Pt, Ni, and Ni-Mo Electrocatalysts for Hydrogen Evolution on Crystalline Si Electrodes. *Energy Environ. Sci.* **2011**, *4*, 3573-3583.

(10) Wang, J.; Xu, F.; Jin, H.; Chen, Y.; Wang, Y. Non-Noble Metal-Based Carbon Composites in Hydrogen Evolution Reaction: Fundamentals to Applications. *Adv. Mater.* **2017**, *29*, 1605838.

(11) Liu, T.; Ma, X.; Liu, D.; Hao, S.; Du, G.; Ma, Y.; Asiri, A. M.; Sun, X.; Chen, L. Mn Doping of CoP Nanosheets Array: An Efficient Electrocatalyst for Hydrogen Evolution Reaction with Enhanced Activity at All pH Values. *ACS Catal.* **2017**, *7*, 98-102.

(12) McKone, J. R.; Marinescu, S. C.; Brunschwig, B. S.; Winkler, J. R.; Gray, H. B. Earth-Abundant Hydrogen Evolution Electrocatalysts. *Chem. Sci.* **2014**, *5*, 865-878.

(13) Liu, H.; He, Q.; Jiang, H.; Lin, Y.; Zhang, Y.; Habib, M.; Chen, S.; Song, L. Electronic Structure Reconfiguration toward Pyrite NiS_2 *via* Engineered Heteroatom Defect Boosting Overall Water Splitting. *ACS Nano* **2017**, *11*, 11574-11583.

(14) Hu, C.; Ma, Q.; Hung, S. -F.; Chen, Z. -N.; Ou, D.; Ren, B.; Chen, H. M.; Fu, G.; Zheng, N. In situ Electrochemical Production of Ultrathin Nickel Nanosheets for Hydrogen Evolution Electrocatalysis. *Chem* **2017**, *3*, 122-133.

(15) Xue, Z. -H.; Su, H.; Yu, Q. -Y.; Zhang, B.; Wang, H. -H.; Li, X. -H.; Chen, J. -S. Janus Co/CoP Nanoparticles as Efficient Mott-Schottky Electrocatalysts for Overall Water Splitting in Wide pH Range. *Adv. Energy Mater.* **2017**, 7, 1602355.

(16) Su, J.; Yang, Y.; Xia, G.; Chen, J.; Jiang, P.; Chen, Q. Ruthenium-Cobalt Nanoalloys Encapsulated in Nitrogen-Doped Graphene as Active Electrocatalysts for Producing Hydrogen in

Alkaline Media. *Nat. Commun.* **2017**, *8*,14969.

(17) Zheng, Y.; Jiao, Y.; Zhu, Y.; Li, L. H.; Han, Y.; Chen, Y.; Jaroniec, M.; Qiao, S. -Z. High Electrocatalytic Hydrogen Evolution Activity of An Anomalous Ruthenium Catalyst. *J. Am. Chem. Soc.* **2016**, *138*, 16174-16181.

(18) Durst, J.; Siebel, A.; Simon, C.; Hasche, F.; Herranz, J.; Gasteiger, H. A. New Insights into the Electrochemical Hydrogen Oxidation and Evolution Reaction Mechanism. *Energy Environ. Sci.* **2014**, *7*, 2255-2260.

(19) Zhang, Y.; Zhou, Q.; Zhu, J.; Yan, Q.; Dou, S. X.; Sun, W. Nanostructured Metal Chalcogenides for Energy Storage and Electrocatalysis. *Adv. Funct. Mater.* **2017**, *27*, 1702317.

(20) Anantharaj, S.; Ede, S. R.; Sakthikumar, K.; Karthick, K.; Mishra, S.; Kundu, S. Recent Trends and Perspectives in Electrochemical Water Splitting with An Emphasis on Sulfide, Selenide, and Phosphide Catalysts of Fe, Co, and Ni: A Review. *ACS Catal.* **2016**, *6*, 8069-8097.

(21) Wang, D. -Y.; Gong, M.; Chou, H. -L.; Pan, C. -J.; Chen, H. -A.; Wu, Y.; Lin, M. -C.; Guan, M.; Yang, J.; Chen, C. -W.; Wang, Y. -L.; Hwang, B. -J.; Chen, C. -C.; Dai, H. Highly Active and Stable Hybrid Catalyst of Cobalt-Doped FeS_2 Nanosheets-Carbon Nanotubes for Hydrogen Evolution Reaction. *J. Am. Chem. Soc.* **2015**, *137*, 1587-1592.

(22) Lu, Q.; Yu, Y.; Ma, Q.; Chen, B.; Zhang, H. 2D Transition-Metal-Dichalcogenide-Nanosheet-Based Composites for Photocatalytic and Electrocatalytic Hydrogen Evolution Reactions. *Adv. Mater.* **2016**, *28*, 1917-1933.

(23) Li, D. J.; Maiti, U. N.; Lim, J.; Choi, D. S.; Lee, W. J.; Oh, Y.; Lee, G. Y.; Kim, S. O. Molybdenum Sulfide/N-Doped CNT Forest Hybrid Catalysts for High-Performance Hydrogen Evolution Reaction. *Nano Lett.* **2014**, *14*, 1228-1233.

(24) Kong, D.; Wang, H.; Cha, J. J.; Pasta, M.; Koski, K. J.; Yao, J.; Cui, Y. Synthesis of MoS_2 and $MoSe_2$ Films with Vertically Aligned Layers. *Nano Lett.* **2013**, *13*, 1341-1347.

(25) Geng, X.; Wu, W.; Li, N.; Sun, W.; Armstrong, J.; Al-hilo, A.; Brozak, M.; Cui, J.; Chen, T. Three-Dimensional Structures of MoS_2 Nanosheets with Ultrahigh Hydrogen Evolution Reaction in Water Reduction. *Adv. Funct. Mater.* **2014**, *24*, 6123-6129.

(26) Wiensch, J. D.; John, J.; Velazquez, J. M.; Torelli, D. A.; Pieterick, A. P.; McDowell, M. T.; Sun, K.; Zhao, X.; Brunschwig, B. S.; Lewis, N. S. Comparative Study in Acidic and Alkaline Media of the Effects of pH and Crystallinity on the Hydrogen-Evolution Reaction on MoS_2 and $MoSe_2$. *ACS Energy Lett.* **2017**, *2*, 2234-2238.

(27) Zhang, J.; Wu, J.; Guo, H.; Chen, W.; Yuan, J.; Martinez, U.; Gupta, G.; Mohite, A.; Ajayan, P. M.; Lou, J. Unveiling Active Sites for the Hydrogen Evolution Reaction on Monolayer MoS_2. *Adv. Mater.* **2017**, *29*, 1701955.

(28) Tsai, C.; Li, H.; Park, S.; Park, J.; Han, H. S.; Nørskov, J. K.; Zheng, X.; Abild-Pedersen, F. Electrochemical Generation of Sulfur Vacancies in the Basal Plane of MoS_2 for Hydrogen Evolution. *Nat. Commun.* **2017**, *8*, 15113.

(29) Voiry, D.; Yamaguchi, H.; Li, J. W.; Silva, R.; Alves, D. C. B.; Fujita, T.; Chen, M. W.; Asefa, T.; Shenoy, V. B.; Eda, G.; Chhowalla, M. Enhanced Catalytic Activity in Strained Chemically Exfoliated WS_2 Nanosheets for Hydrogen Evolution. *Nat. Mater.* **2013**, *12*, 850-855.

(30) Dou, S.; Tao, L.; Huo, J.; Wang, S.; Dai, L. Etched and Doped Co_9S_8/Graphene Hybrid for Oxygen Electrocatalysis. *Energy Environ. Sci.* **2016**, *9*, 1320-1326.

(31) Huang, Z. -F.; Song, J.; Li, K.; Tahir, M.; Wang, Y. -T.; Pan, L.; Wang, L.; Zhang, X.; Zou, J. -J. Hollow Cobalt-Based Bimetallic Sulfide Polyhedra for Efficient All-pH-Value Electrochemical

and Photocatalytic Hydrogen Evolution. *J. Am. Chem. Soc.* **2016**, *138*, 1359-1365.

(32) Faber, M. S.; Lukowski, M. A.; Ding, Q.; Kaiser, N. S.; Jin, S. Earth-Abundant Metal Pyrites (FeS_2, CoS_2, NiS_2, and Their Alloys) for Highly Efficient Hydrogen Evolution and Polysulfide Reduction Electrocatalysis. *J. Phys. Chem. C* **2014**, *118*, 21347-21356.

(33) Faber, M. S.; Dziedzic, R.; Lukowski, M. A.; Kaiser, N. S.; Ding, Q.; Jin, S. High-Performance Electrocatalysis Using Metallic Cobalt Pyrite (CoS_2) Micro- and Nanostructures. *J. Am. Chem. Soc.* **2014**, *136*, 10053-10061.

(34) Lacroix, M.; Boutarfa, N.; Guillard, C.; Vrinat, M.; Breysse, M. Hydrogenating Properties of Unsupported Transition Metal Sulfides. *J. Catal.* **1989**, *120*, 473-477.

(35) Liu, P.; Rodriguez, J. A.; Asakura, T.; Gomes, J.; Nakamura, K. J. Desulfurization Reactions on Ni_2P (001) and α-Mo_2C (001) Surfaces: Complex Role of P and C Sites. *Phys. Chem. B* **2005**, *109*, 4575-4583.

(36) Popczun, E. J.; McKone, J. R.; Read, C. G.; Biacchi, A. J.; Wiltrout, A. M.; Lewis, N. S.; Schaak, R. E. Nanostructured Nickel Phosphide as An Electrocatalyst for the Hydrogen Evolution Reaction. *J. Am. Chem. Soc.* **2013**, *135*, 9267-9270.

(37) Liang, H.; Gandi, A. N.; Xia, C.; Hedhili, M. N.; Anjum, D. H.; Schwingenschlögl, U.; Alshareef, H. N. Amorphous NiFe-OH/NiFeP Electrocatalyst Fabricated at Low Temperature for Water Oxidation Applications. *ACS Energy Lett.* **2017**, *2*, 1035-1042.

(38) Chen, S.; Duan, J.; Tang, Y.; Jin, B.; Qiao, S. Molybdenum Sulfide Clusters-Nitrogen-Doped Graphene Hybrid Hydrogel Film as An Efficient Three-Dimensional Hydrogen Evolution Electrocatalyst. *Nano Energy* **2015**, *11*, 11-18.

(39) Ganesan, P.; Prabu, M.; Sanetuntikul, J.; Shanmugam, S. Cobalt Sulfide Nanoparticles Grown

on Nitrogen and Sulfur Codoped Graphene Oxide: An Efficient Electrocatalyst for Oxygen Reduction and Evolution Reactions. *ACS Catal.* **2015**, 5, 3625-3637.

(40) Ferrari, A. C.; Basko, D. M. Raman Spectroscopy as A Versatile Tool for Studying the Properties of Graphene. *Nat. Nanotechnol.* **2013**, *8*, 235-246.

(41) Matsumoto, K.; Matsumoto, T.; Kawano, M.; Ohnuki, H.; Shichi, Y.; Nishide, T.; Sato, T. Syntheses and Crystal Structures of Disulfide-Bridged Binuclear Ruthenium Compounds: the First UV-Vis, Raman, ESR, and XPS Spectroscopic Characterization of A Valence-Averaged Mixed-Valent $Ru^{III}SSRu^{II}$ Core. *J. Am. Chem. Soc.* **1996**, *118*, 3597-3609.

(42) Shervedani, R. K.; Amini, A. Sulfur-Doped Graphene as A Catalyst Support: Influences of Carbon Black and Ruthenium Nanoparticles on the Hydrogen Evolution Reaction Performance. *Carbon* **2015**, *93*, 762-773.

(43) Ito, Y.; Cong, W.; Fujita, T.; Tang, Z.; Chen, M. High Catalytic Activity of Nitrogen and Sulfur Co-Doped Nanoporous Graphene in the Hydrogen Evolution Reaction. *Angew. Chem.* **2015**, *127*, 2159-2164.

(44) Ma, Q.; Hu, C.; Liu, K.; Hung, S. -F.; Ou, D.; Chen, H. M.; Fu, G.; Zheng, N. Identifying the Electrocatalytic Sites of Nickel Disulfide in Alkaline Hydrogen Evolution Reaction. *Nano Energy* **2017**, *41*, 148-153.

(45) Wu, Y.; Liu, Y.; Li, G. -D.; Zou, X.; Lian, X.; Wang, D.; Sun, L.; Asefa, T.; Zou, X. Efficient Electrocatalysis of Overall Water Splitting by Ultrasmall $Ni_xCo_{3-x}S_4$ Coupled Ni_3S_2 Nanosheet Arrays. *Nano Energy* **2017**, *35*, 161-170.

(46) Zhang, H.; Li, Y.; Zhang, G.; Wan, P.; Xu, T.; Wu, X.; Sun, X. Highly Crystallized Cubic Cattierite CoS_2 for Electrochemically Hydrogen Evolution over Wide pH Range from 0 to 14.

Electrochim. Acta **2014**, *148*, 170-174.

(47) Pu, Z.; Liu, Q.; Asiri, A. M.; Luo, Y.; Sun, X.; He, Y. 3D Macroporous MoS_2 Thin Film: in situ Hydrothermal Preparation and Application as A Highly Active Hydrogen Evolution Electrocatalyst at All pH Values. *Electrochim. Acta* **2015**, *168*, 133-138.

(48) Wu, Z.; Guo, J.; Wang, J.; Liu, R.; Xiao, W.; Xuan, C.; Xia, K.; Wang, D. Hierarchically Porous Electrocatalyst with Vertically Aligned Defect-Rich CoMoS Nanosheets for the Hydrogen Evolution Reaction in An Alkaline Medium. *ACS Appl. Mater. Interfaces* **2017**, *9*, 5288-5294.

(49) Yang, Y.; Zhang, K.; Lin, H.; Li, X.; Chan, H. C.; Yang, L.; Gao, Q. MoS_2-Ni_3S_2 Heteronanorods as Efficient and Stable Bifunctional Electrocatalysts for Overall Water Splitting. *ACS Catal.* **2017**, *7*, 2357-2366.

(50) Kuang, P.; Tong, T.; Fan, K.; Yu, J. In situ Fabrication of Ni-Mo Bimetal Sulfide Hybrid as An Efficient Electrocatalyst for Hydrogen Evolution over a Wide pH Range. *ACS Catal.* **2017**, *7*, 6179-6187.

(51) Wang, J.; Zhong, H.; Wang, Z.; Meng, F.; Zhang, X. Integrated Three-Dimensional Carbon Paper/Carbon Tubes/Cobalt-Sulfide Sheets as An Efficient Electrode for Overall Water Splitting. *ACS Nano* **2016**, *10*, 2342-2348.

(52) Tian, T.; Huang, L.; Ai, L.; Jiang, J. Surface Anion-Rich NiS_2 Hollow Microspheres Derived from Metal-Organic Frameworks as A Robust Electrocatalyst for the Hydrogen Evolution Reaction. *J. Mater. Chem. A* **2017**, *5*, 20985-20992.

(53) Morales-Guio, C. G.; Liardet, L.; Mayer, M. T.; Tilley, S. D.; Gratzel, M.; Hu, X. Photoelectrochemical Hydrogen Production in Alkaline Solutions Using Cu_2O Coated with Earth-Abundant Hydrogen Evolution Catalysts. *Angew. Chem. Int. Ed.* **2015**, *54*, 664-667.

(54) Barman, B. K.; Das, D.; Nanda, K. K. Facile Synthesis of Ultrafine Ru Nanocrystal Supported N-Doped Graphene as An Exceptional Hydrogen Evolution Electrocatalyst in Both Alkaline and Acidic Media. *Sustainable Energy Fuels*, **2017**, *1*, 1028-1033.

(55) McKone, J. R.; Sadtler, B. F.; Werlang, C. A.; Lewis, N. S.; Gray, H. B. Ni-Mo Nanopowders for Efficient Electrochemical Hydrogen Evolution. *ACS Catal.* **2013**, *3*, 166-169.

(56) Yin, J.; Fan, Q.; Li, Y.; Cheng, F.; Zhou, P.; Xi, P.; Sun, S. Ni-C-N Nanosheets as Catalyst for Hydrogen Evolution Reaction. *J. Am. Chem. Soc.* **2016**, *138*, 14546-14549.

(57) Laursen, A. B.; Patraju, K. R.; Whitaker, M. J.; Retuerto, M.; Sarkar, T.; Yao, N.; Ramanujachary, K. V.; Greenblatt, M.; Dismukes, G. C. Nanocrystalline Ni_5P_4: A Hydrogen Evolution Electrocatalyst of Exceptional Efficiency in Both Alkaline and Acidic Media. *Energy Environ. Sci.* **2015**, *8*, 1027-1034.

(58) Ma, L.; Ting, L. R. L.; Molinari, V.; Giordano, C.; Yeo, B. S. Efficient Hydrogen Evolution Reaction Catalyzed by Molybdenum Carbide and Molybdenum Nitride Nanocatalysts Synthesized via the Urea Glass Route. *J. Mater. Chem. A* **2015**, *3*, 8361-8368.

(59) Fang, Y. H.; Liu, Z. P. Mechanism and Tafel Lines of Electro-Oxidation of Water to Oxygen on RuO_2(110). *J. Am. Chem. Soc.* **2010**, *132*, 18214-18222.

(60) Wang, P.; Zhang, X.; Zhang, J.; Wan, S.; Guo, S.; Lu, G.; Yao, J.; Huang, X. Precise Tuning in Platinum-Nickel/Nickel Sulfide Interface Nanowires for Synergistic Hydrogen Evolution Catalysis. *Nat. Commun.* **2017**, *8*, 14580.

TOC:

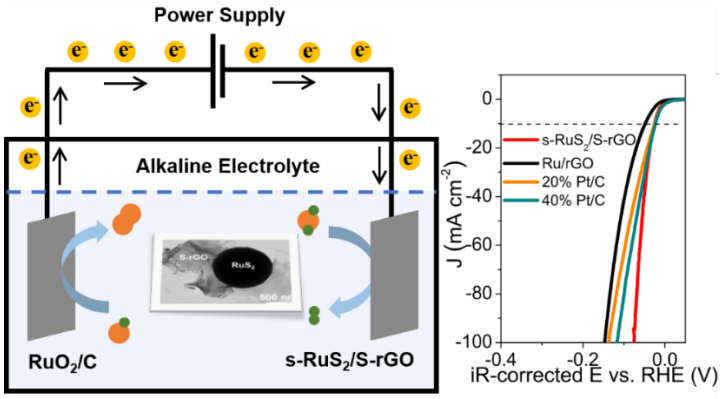
Power Supply
Alkaline Electrolyte
RuO2/C
s-RuS2/S-rGO
s-RuS2/S-rGO
Ru/rGO
20% Pt/C
40% Pt/C
J (mA cm-2)
iR-corrected E vs. RHE (V)
0
-20
-40
-60
-80
-100
-0.4
-0.2
0.0